**Atmospheric
Chemistry
and Physics
Discussions**

Characterization of ions at Alpine waterfalls

P. Kolarž[1,*], M. Gaisberger[2,*], P. Madl[3], W. Hofmann[3], M. Ritter[2], and A. Hartl[2]

[1]Institute of Physics, University of Belgrade, Pregrevica 118, 11080 Belgrade, Serbia
[2]Paracelsus Medical University, Institute for Physiology and Pathophysiology, Strubergasse 21, 5020 Salzburg, Austria
[3]University of Salzburg, Department of Materials Research and Physics, Division of Physics and Biophysics, Hellbrunner Str. 34, 5020 Salzburg, Austria
[*]These authors contributed equally to this work.

Correspondence to: P. Kolarž (kolarz@ipb.ac.rs)

ACPD

11, 25297–25325, 2011

Characterization of ions at Alpine waterfalls

P. Kolarž et al.

Title Page

Abstract	Introduction
Conclusions	References
Tables	Figures

|◄ | ►|
| ◄ | ► |

Back | Close

Full Screen / Esc

Printer-friendly Version

Interactive Discussion

Abstract

During a three-year field campaign of measuring waterfall generated ions, we monitored five different waterfalls in the Austrian Alps. Most measurements were performed at the Krimml waterfall (Salzburg), which is the biggest and most visited one in Europe and the Gartl waterfall (Mölltal, Carinthia). Smallest ion sizes (0.9–2 nm) were measured with a cylindrical air ion detector (CDI-06) while ion sizes from 5.5 to 350 nm were measured using a modified Grimm SMPS aerosol spectrometer. Measurements showed high negative ion gradients nearby waterfalls whereas positive ions showed only a moderate increase. The most abundant sizes of nano-sized and sub-micrometer ions measured were at 2 nm and of the larger and heavier ones at 120 nm.

1 Introduction

1.1 Air ions in the environment

The term "air ions" refers to all charged airborne particles that have electrical mobility. In general, they are continually created by natural sources such as cosmic rays, radioactive decay of noble gases (such as radon) in the air and radioactive minerals from the ground. After the ionization process and in a very short time (typically microseconds) primary ions evolve via a process of hydration and ion cluster formation into complexes known as small air ions (charged nano-aerosols) with a lifetime of up to 100 s. The central ion of a cluster could contain one inorganic molecule and be surrounded by one layer of water molecules. However, due to the purity of the water, such inoculation cores are largely absent in the aerosols of the waterfalls (WF) investigated. The background concentration of air ions in the environment is about a few hundred per cubic centimetre with an average near-ground ionization rate of 10 ion pairs $cm^{-3} s^{-1}$.

Title Page

Abstract | Introduction

Conclusions | References

Tables | Figures

◄ | ►|

◄ | ►

Back | Close

Full Screen / Esc

Printer-friendly Version

Interactive Discussion

The ion concentration ($n^\pm$) itself is determined by the following balance equation:

$$\frac{dn^\pm}{dt} = q - \alpha n^\pm n^\mp - n^\pm \beta Z \tag{1}$$

where q is the volumetric production rate, Z is the aerosol number concentration and α, β account for the losses of ion to ion recombination and ion-aerosol attachment.

⁵ Mobility of the positive air ions is lower (as the diameter is larger) resulting in a higher neutralization coefficient β of negative ions and consequently yields lower concentrations in the natural surroundings (Eq. 1). The average ratio of positive and negative ion concentrations, i.e. the unipolarity coefficient, in natural surroundings is $n^+/n^- = 1.12$ (Hõrrak, 2001).

¹⁰ According to the size categorization provided by Hõrrak (2001), air ions are classified in small (sub-nano-sized 0.42–0.85 nm), big clusters (nano-sized 0.85–1.6 nm), intermediate (1.6–7.5 nm), light large (7.5–22 nm) and heavy large (sub-micrometer 22–79 nm) clusters. Intermediate and large ions are also called aerosol ions (Hõrrak et al., 1994). Air ions are supposed to carry only a single elementary charge that relates

¹⁵ mobility with mass if the carrier gas is known (Aplin, 2008). The relationship between ion radius and mobility was calculated using the algorithm given by Tammet (1995).

There are many natural and artificial mechanisms of air ion generation in the environment. In this study, we investigated the "waterfall effect", which creates mostly negative ions, also known as Lenard's ions (Lenard, 1892). Upon creation, WF droplets

²⁰ undergo charge redistribution forming dipoles with negatively charged surfaces. The phenomenon of charge separation occurs as a consequence of disruption of the water surface by splashing and bubbling when moving liquid is aerosolized at an obstacle or by aerodynamic break-up of water droplets during free fall (see Fig. 1). After break-up by whatever mechanism, smaller fragments (or clusters) are carrying negatively

²⁵ charged OH$^-$ ions, while the remaining bigger fragments are positive where large proton clusters are known as $H_3O^+(H_2O)_{20}$ (Parts et al., 2007; Luts et al., 2009; Hulthe et al., 1997; Vostrikov et al., 2006). A positive value of droplet surface potential (+0.1 V) indicates that the water dipoles are preferentially oriented with the negative pole toward

Characterization of ions at Alpine waterfalls

P. Kolarž et al.

Title Page

Abstract | Introduction

Conclusions | References

Tables | Figures

|◄ | ►|

◄ | ►

Back | Close

Full Screen / Esc

Printer-friendly Version

Interactive Discussion

P. Kolarž et al.

the gas phase while the positive pole is oriented towards the liquid phase (Parfenyuk, 2002).

$(H_2O)_n \rightarrow (H_3O^+)(H_2O)_{n-m} + OH^-(H_2O)_{m-2}$ where $m \gg n$.
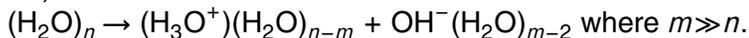
Botti et al. (2004) suggested that OH^- ions are hydrated with 4 H_2O molecules with a presence of a weakly bound fifth water molecule close to the hydrogen atoms. Negatively charged particles remain in the air and become thermophoretically dispersed due to the cold air stream caused by the temperature difference of the water and the surrounding air. The larger positively charged droplets precipitate to the ground, i.e. in the pond. As a result, negative air ion concentrations near WFs easily reach several tens of thousands per cubic centimetre.

Laakso et al. (2007) found that the diameter of WF-related negative air ions range between 1.5–10 nm, whereby 2 nm sized negative ions were most abundant.

Physiological and medical effects of ions and waterfalls has been described (Iwama, 2004; Yamada et al., 2005; Takahashi et al., 2008), but interpretation of specific health related effects still require a thorough physical characterization, especially when related to waterfalls.

2 Methods

2.1 Instrumentation and measurements

Ion concentrations of 0.9, 1.5, 2 nm diameter were measured using 3 identical air ion detectors (CDI-06) based on the aspirated Gerdien condenser principle (Gerdien, 1905), made in the Institute of Physics, Belgrade. All detectors have their own power supply, temperature, pressure and relative humidity sensors, and also features such as dynamic zeroing, live data acquisition, with programmable data averaging, sampling and polarity change (Kolarž et al., 2005, 2009). The critical mobility (μ_c), i.e. the smallest ion mobility to be measured (maximum size), is defined as a combination of

polarizing voltage (U) and air flow:

$$\mu_c = \frac{V_S \left(R_2^2 - R_1^2 \right) \ln \left(R_2 / R_1 \right)}{2\,L\,U} \qquad (2)$$

where R_2 and R_1 are the radii of the polarizing and collecting electrode; L is the collecting electrode length and V_S is the air velocity through the electrodes. Air-flow and
polarizing voltage on 3 detectors were set to measure air ions in size ranges $\leq$0.9, 1.5
and 2 nm (Eq. 2). These three values are depicted due to characteristic sizes of ions
created by WF, which is around 2 nm (Laakso et al., 2007) and by nuclear decay as well
as cosmic rays – with the latter up to 0.9 nm. It is expected that simultaneous measurements of all three instruments on places where no WF-related ions are present should
show approximate air ion concentrations. The instrumental uncertainties under regular
conditions are about 5 % (Kolarž et al., 2009). Taking into account the extreme and
difficult conditions during the field campaign and particularly near the WFs, an additional uncertainty should be added. Yet, efforts, such as maintaining constant RPM
of the fans, thermostated electronics and electrodes, use of additional protective case
and manual zeroing procedure have been employed to limit uncertainties to additional
10 %. Altogether, by using the "root-sum-of-squares" method the overall uncertainty
amounts to 11 %.

Air ion particles in the size range from 5.5 to 358 nm were measured with the
Grimm SMPS (Scanning Mobility Particle Sizer) using an M-DMA (Medium-Differential
Mobility Analyzer) for size class differentiation and an attached CPC (Condensation
Particle Counter) to quantify the particle concentration. Within the DMA, the particles are selected according to their electrical mobility, which is accomplished using
a [241]Am radioactive source mounted on the DMA air inlet. To avoid neutralization of
the aerosolised ions, this so-called "neutralizer" was detached from the M-DMA. Doing
so one obtains an SMPS detector that is able to count negatively charged particles.
The entire system was operated with a backup battery power supply enabling 8 h of
uninterrupted operation in the field.

Characterization of ions at Alpine waterfalls

P. Kolarž et al.

Title Page

Abstract	Introduction
Conclusions	References
Tables	Figures

|◄ | ►|
◄ | ►

Back | Close

Full Screen / Esc

Printer-friendly Version

Interactive Discussion

Atmospheric data like temperature and wind speed were measured by a PCE-007 anemometer attached to a data logger.

Measurement of ion concentrations in the vicinity of the WF is difficult and restricted due to the existence of dispersed drops in the air (water aerosols). These droplets are not only contributing to the increase in relative humidity but also in wetting the instruments, soaking the electrodes of the CDI, thereby causing current leakages in the electrode system and amplifying electronics.

In addition, the temperature gradient at the falls results in a heavy surge, which is directed away from the WF downstream in periodical gusts – especially at the Krimml WF. These gusts are carrying water aerosols, and are usually, but not always, higher loaded with air ions. Periods of intense gusts are followed by modest ones and typically last for a few tens of seconds.

These conditions limit the duration of the measurements and act as a delimiting factor when attempting to obtain a comprehensive outline of the inventory at the falls. All these difficulties were partially avoided by encasing the CDI instruments in aluminium boxes with inlets for the probes and outlet for exhaust and excess heat. These cases also contributed to the protection of control- and supply units. The SMPS was also operated in a sealed housing, thus only the inlet was subject to excessive humidity. All instruments were mounted onto a 4-wheel trolley fitted with a tow rail (Fig. 2). It is small enough to be loaded onto a pick-up truck in order to approach different falls at different off-road locations.

3 Measurements and discussion

3.1 Study of 5 different WFs

During the summer of 2008, five WFs in Austria were studied and compared with control sites where WF-related ions were not present. Table 1 shows average and maximal number concentrations of positive and negative air ions of 4 alpine and one artificial

WF. All WF ion concentrations were measured at places of maximal ionization and moderate wetting of the instruments. The highest average concentration increase of 2 nm-sized negative ions – in comparison to control point's concentration – was found to be 80-fold.

5   WF ion concentrations fluctuate depending on measuring sites, but their averages at the examined sites typically depend on the quantity of water flow, which varies seasonally. In contrast, the origin and structure of the ions generated at reference sites arise mostly from natural radioactivity, which is subject to diurnal changes (Kolarž et al., 2009; Chandrashekara, et al., 2006). Accordingly, the presented relations between

10 WF and background ions vary diurnally and seasonally.

The data in Table 1 lead to the conclusion that the production of WF ions not only depends on the height of the WF and its quantity of water flowing per unit of time, but also on the location of the WF, the surrounding topography, and of course, the location of the measuring points.

15 Larger WFs create periodical gusts, which are usually carrying a lot of water droplets that can be seen with the naked eye and likewise felt on the skin. These gusts do not necessarily carry small water droplets but when they do, the resulting increase in concentration of WF-generated ions are immediately detected by the instruments. This is especially significant at the Krimml WF where three falling cascades generate very

20 complex air-flow patterns.

Figure 3 shows the artificial WF with a cascade that is 5 m high on the river Möll. Although ion concentrations are 11-fold higher than background measurements, they are much lower than any of the higher WFs (Table 1). This supports the assumption that one of the processes that contribute to WF ion generation is charge separation

25 via aerodynamic break-up of micrometer-sized water droplets into nano-sized aerosols (Zilch et al., 2008). Another mechanism regards the rapid decline in relative humidity as the aerosolised droplets drift further off the WF. This implies that if the particle size is larger than the Kelvin diameter, the aerosol particles will grow; if the particle size is smaller, they will evaporate.

Hence, as one moves away from the waterfall and due to the change in super-saturated conditions, the corresponding Kelvin droplet diameter becomes larger as under-saturated conditions are reached (decrease in relative humidity and increase in temperature), which causes the aerosols to shrink in size, further accounting to a

5   smaller particle sized diameter. However, the most prominent mechanism of formation is encountered when the water droplets hit a surface (water, or rock), thereby fragment and in combination with the above (bubble bursting effect, as shown in Fig. 1) yield nano-sized aerosols.

3.2   Ion inventory at the Krimml WF

10   The Krimml WF is located in the northern region of the "Hohe Tauern" – a part of the eastern alpine region. It belongs to a glacial creek named "Krimmler Ache" whose water flows according to the season. In July the average throughput is about $20\,000\,\mathrm{m^3\,h^{-1}}$, whereas it is only $500\,\mathrm{m^3\,h^{-1}}$ in February. The WF itself consists of three consecutive cascades, with a height of 140 m, 100 m and 140 m high (Fig. 4). The base

15   of the WF is at an altitude of around 1100 m above sea level. The height of the last WF cascade provides maximal velocity to water droplets as the flow reaches $53\,\mathrm{m\,s^{-1}}$. The chemical composition of the water reveals an almost neutral pH (7.36) with very low concentrations of Ca^{2+} ($3.45\,\mathrm{mg\,L^{-1}}$), Mg^{2+} ($1.22\,\mathrm{mg\,L^{-1}}$) and Cl^- ($0.26\,\mathrm{mg\,L^{-1}}$). The conductivity was $30\,\mathrm{\mu S\,cm^{-1}}$.

20   From a microbiological point of view, the water quality showed a moderate enraged count of colony forming units ($100\,\mathrm{CFU\,ml^{-1}}$). Simultaneous measurements of small clusters, intermediate and large ions created by the WF and natural ionizing radiation were performed – shown in Fig. 4 – over a two-week period in July 2010 on both sides of the bottom cascade at the Krimml WF.

25   To test the performance of the instrumentation, an inter-comparison between the cylindrical ion detectors was done (Fig. 5). Two detectors, with the same voltage and amplification settings, placed side by side, were used to measure negative ion concentration gradients near the Krimml WF. For that purpose, the trolley (Fig. 2) was used

for translocation among the various sampling sites and for the slow approach to the nearest point of the orographic right side at the falls. The Figure reveals the Pearson correlation factor of $r = 0.97$, which is more than satisfactory considering the measuring conditions encountered during the campaign (Fig. 5). Testing was conducted also at different sites and locations.

Gradients of ≤ 2 nm size positive and negative air ion concentrations measured during the three-week field campaign at the Krimml WFs in July 2010 are shown in Fig. 6. Distances were measured from the base of the lowest cascade (using Google earth coordinates: 47.208283 N/12.170859 E). On the orographic right side, with the last measuring points being the reference site some 547 m away from the falls, assuming that no WF-related ions are present there. The reason for the relatively short gradient distance on the orographic left side is due to the dense forest cover that dominates the farther site some 228 m from the WF. The differences between the maximal values on the left and the right side of the WF, i.e. the creek, arise from the topographic configuration, the time variations when measurements were performed, turbulent air flows and varied solar flux within the upper Krimml valley.

All ion measurements were carried out at points that ensure that the instruments were not subject to instant flooding. Accordingly, the nearest measuring points were 57 m and 75 m on the orographic left and right side of the Krimml WF, respectively. Both measuring points are slightly shifted out of the main axis, which is directed sharply to the left orographic uphill side (Fig. 4 and aerial view of Fig. 6). The lower concentration on the left side is the result of complex turbulent air-flow generated by the huge amount of water pouring into the pond.

In comparison with the other WFs that we measured (Table 1), the maximal ion concentrations generated near the Krimml WF were apparently low, i.e. only about 20 times higher than the measured background, while maximal ion concentrations at the Gartl WF (Döllach) amounted to 6×10^4 ions cm^{-3}, i.e. 120 times higher than the measured background. Noteworthy for our field observation is that although the Krimml WF generates much more aerosols but fewer in the sub-nano-size range, wetting of

the instrumentation is much more prevalent than at the other WFs. Due to the dynamics of waterfall generated aerosols, monitoring the inventory with a SMPS is not the first choice, as it requires a 120 s interval for the completion of a full scan. The ideal detector should at least measure in seconds intervals, like the ELPI. However this instrument – due to its weight and power requirements – makes field measurements a real challenge. In order to overcome this shortage, at least 3 full SMPS scans were made at every point, each divided into 44 size channels and each channel computed as an average of 9 individual recordings (out of which the 1st and the 9th are omitted as the system dynamically changes the voltage when switching from one size bin to the next). Using the SMPS and due to the nature of its detection principle it measures only negatively charged particles. Consequently, it deprived us from the ability to monitor the increase of positively charged aerosols in the 200 nm size range and beyond, as reported by Reiter (1994).

3.3 Ion measurements at the Krimml WF

Gradients of 0.9, 1.5 and 2 nm size positive and negative integral ion concentrations are shown in Fig. 7. As mentioned before, the non-linear decay function of the negative ion concentration is caused by the local topography and wind patterns. Positive ions did not reveal significant increases in concentrations and only 2 nm sized ions showed a nice correlation ($r = 0.6$) between positive and negative ions gradients. Interestingly enough, all three dimensions of positive ions were rising with distance within the first hundred meters from the waterfall only to decrease further afield. This is probably due to very high concentrations of negative ions as well as aerosols in the vicinity of the waterfall. This implies that higher coefficients of α and β (see Eq. 1) amplified by strong turbulent air flow patterns must be taken into consideration.

Equalization of the smallest positive and negative air ion concentrations is a signal that almost all WF-related negative ions are neutralized. The remaining ones can be traced back to the formation mechanisms usually associated to natural radioactivity and cosmic radiation. This is the case at the last point ($l = 547$ m) downstream from the WF

visible in Figs. 7, 8, 9. The average wind speed from the first to the last point measured was $4.6\,\mathrm{m\,s^{-1}}$. Approximate calculations showed that under these circumstances, WF-related ions could persist up to 120 s.

Supplementary measurements done at various locations showed radon concentrations in the water above and below the Krimml WF to be 141 and $148\,\mathrm{Bq\,m^{-3}}$, respectively (measured with a RAD-7 instrument, Durridge Co, USA), hence they remain neglected for the overall ion production rate. Also, natural radioactivity in the air was measured with a Gamma Scout counter showing typical background values of $\sim0.15\,\mathrm{mSv\,h^{-1}}$. As outlined in the "Methods", the particle diameter range from 0.9 to 350.4 nm was measured using CDI-06 and modified SMPS with M-DMA at 5 measuring points (Fig. 9).

The air ion concentration peak at the reference point (547 m) is slightly shifted to smaller ion sizes and as outlined above, as a result of different source and formation mechanisms. Air ions created by ionizing radiation are smaller than WF-related ions. Their size range is shown by the reference point data series (547 m) where 0.9 nm ions were the most abundant.

According to Laakso et al. (2007), the ion-effect of the WF is visible only in ions smaller than approximately 30 nm with a maximal rise of negative ions concentration near the WF in the size range of 1.5 to 10 nm. Our measurements showed that WF-generated ions up to 25 nm with a corresponding maximal concentration increase measured at 2 nm – which assorts well with Laakso et al. (2007) – in particular when keeping in mind the differences arising from measuring conditions, temperature and size of the WF.

In the size range between 25 and 40 nm there is no increase in observable WF-generated ions, whereas larger ions are present from 40 to above 350 nm, whereby clustering took place into a size window at around 120 nm. Here the WF-related ion concentration is approximately 3-fold higher than at the reference site some 547 m away from the Krimml WF. The observed increase of 0.9 nm ions at close range to the falls is also remarkable as it highlights the extended spectrum of the WF-related ion

size range along with its mobility.

3.4 Ion measurements at the Gartl WF

The Gartl WF – as shown in Fig. 10 – is located in the southern sector of the "Hohe Tauern" region and is also part of the central eastern inner alpine region. It is composed of 2 cascades that together are about 50 m high and steeply precipitating to the pond at the base of the falls. This WF is tightly embedded into a narrow topographic setting, encompassing a small valley opening and thereby closely surrounded with high cliffs, which are directing the air stream downhill.

The generated ion gradients at Gartl WF show similar trends as observed at Krimml WF. However with significantly higher ion concentrations than at Krimml WF, despite the moderate wind that was prevailing in the direction out of the narrow valley, which reduces the concentration of WF generated ions.

Unlike Krimml WF, the positive ion concentrations at Gartl WF revealed a similar trend as for documented negative ions, but still with an 18 fold lower concentration in the vicinity of the fall itself. As a result, strong correlation factors between same-sized positive and negative ions ($r \sim 0.8$) were obtained (Fig. 11) but with huge deviations in overall concentration. The ratio between negative and positive gradients of ions is shown in Fig. 12, where slightly increased background concentrations of both air ion polarities could be observed (point at 120 m).

Figure 13 depicts the negative ion concentrations vs. aerosol size measured at Gartl WF. It likewise reveals a similar size distribution as observed at Krimml WF (compare with Fig. 9). This very satisfying observation is striking as there is a significant difference in both the topography and the height of the falls. The reference site was located near the Döllach village (Carinthia), a few kilometres aside the falls on the opposite side of the valley.

Characterization of ions at Alpine waterfalls

P. Kolarž et al.

4   Conclusion

Concentrations and size distributions of WF-generated ions in the size range from 0.9 to 350 nm were measured at 2 WFs in the Austrian Alps using a Gerdian-type ion counter and a Scanning Mobility Particle Sizer adapted for ion counting purposes. The
5   WFs herein studied reveal totally different topographical settings, yet their ion size distribution was found to be almost identical and in very good agreement with Laakso et al. (2007). The abundance of negative nano-sized and intermediate ions generated by these WFs was found to be in the size range of 0.2–25 nm with a maximal concentration peak measured at 2 nm. On the other hand, heavier sub-micrometer ions in the
10   range of 40 to 350 nm peaked in a size window at around 120 nm. The generation of 1.5 nm ions was less dominant than those at 0.9 and 2.0 nm.

Positive ions are also generated by these WFs, and their concentrations also differ at each WF; a fact that can most likely be ascribed to the increase of the recombination coefficient α (refer to Eq.1). Measurements at these various WFs show that the number
15   of generated ions depends on numerous parameters such as topographic configuration (surrounding cliffs), quantity of water, altitude, weather and prevailing humidity levels. These parameters determine the quantity of aerosolised water in the form of the ion neutralization coefficient. Compared with the measurements from the artificial WF, we can conclude that bubble break-up on solid surfaces along with splashing of water on
20   aqueous surfaces is a major ionizing source and exceeds the aero dynamic break-up of larger water droplets by far.

References

Aplin, K. L.: Composition and measurement of charged atmospheric clusters, Space Sci. Rev., 137, 213–224, 2008.

Botti, A., Bruni, F., Imberti, S., Ricci, M. A., and Soper, A. K.: Solvation shell of OH$^-$ ions in water, J. Mol. Liq., 117, 81–84, 2004.

Chandrashekara, M. S., Sannapp, J., and Paramesh, L.: Studies on atmospheric electrical conductivity related to ^{222}Rn and its progeny concentrations in the lower atmosphere at Mysore, Atmos. Environ., 40, 87–89, 2006.

Gerdien, H.: Demonstration eines Apparates zur absoluten Messung der elektrischen Leitfahigheit der Luft, Phys. Zeitung, 6, 800–801, 1905.

Hõrrak, U.: Air ion mobility spectrum at a rural area. Dissertationes Geophysicales Universitat Tartuensis, Tartu, Estonia, 2001.

Hõrrak, U., Iher, H., Luts, A., Salm, J., and Tammet, H.: Mobility spectrum of air ions at Tahkuse Observatory, J. Geophys. Res., 99, 10697–10700, 1994.

Hulthe, G., Stenhagen, G., Wennerström, O., Ottosson, CH.: Water clusters studied by electrospray mass spectrometry, J. Chromatogr. A., 777, 155–165, 1997.

Iwama, H.: Negative air ions created by water shearing improve erythrocyte deformity and aerobic metabolism, Indoor Air, 14, 293–297, 2004.

Laakso, L., Hirsikko, A., Gronholm, T., Kulmala, M., Luts, A., and Parts, T.-E.: WFs as sources of small charged aerosol particles, Atmos. Chem. Phys., 7, 2271–2275, doi:10.5194/acp-7-2271-2007, 2007.

Lenard, P.: Über die Elektrizität der Wasserfälle, Ann Phys (Leipz), 46,584-636, 1892.

Luts, A., Parts, T., Laakso, L., Hirsikko, A., Grönholm, T., and Kulmala, M.: Some air electricity phenomena caused by WFs, Correlative study of the spectra, Atmos. Res., 91, 229–237, 2009.

Kolarž, P., Filipovi, D., and Marinkovi, B.: Daily variations of indoor air-ion and radon concentrations, Appl. Radiat. Isotopes, 67, 2062–2067, 2009.

Kolarž, P., Filipovi, D., Marinkovi, B.: Zeroing and testing units developed for Gerdien atmospheric ion detectors, Rev. Sci. Instrum., 76, 046107, 2005.

Parfenyuk, V. I.: Surface potential at the gas-aqueous solution interface, Colloid J., 64, 588–595, 2002.

Parts, T., Luts, A., Laakso, L., Hirsikko, A., Grönholm, T., and Kulmala, M.: Chemical compo-

sition of waterfall-induced air ions, spectrometry vs. simulations, Boreal. Environ. Res., 12, 409–420, 2007.

Reiter, R.: Charges on particles of different size from bubbles of Mediterranean Sea surf and from waterfalls, J. Geophys. Res., 99(D5), 10807–10812, 1994.

Takahashi, K., Otsuki, T., Mase, A., Kawado, T., Kotani, M., Ami, K., Matsushima, H., Nishimura, Y., Miura, Y., Murakami, S., Maeda, M., Hayashi, H., Kumagai, N., Shirahama, T., Yoshimatsu, M., and Morimoto, K.: Negatively-charged air conditions and responses of the human psycho-neuro-endocrino-immune network, Environ. Int., 34(6), 765–772, 2008.

Tammet, H.: Size and mobility of atmospheric particles, clusters and ions, J. Aerosol. Sci., 26, 459–475, 1995.

Yamada, R., Yanoma, S., Akaike, M., Tsuburaya, A., Sugimasa, Y., Takemiya, S., Motohashi, H., Rino, Y., Takanashi, Y., and Imada, T.: Water-generated negative air ions activate NK cell and inhibit carcinogenesis in mice, Cancer Lett., 239, 190–197, 2005.

Vostrikov, A. A., Drozdov, S. V., Rudnev, V. S., and Kurkina, L. I.: Molecular dynamics study of neutral and charged water clusters, Comput. Mater. Sci., 35, 254–260, 2006.

Zilch, L., Maze, J., Smith, J., Ewing, G., and Jarrold, M.: Charge separation in the aerodynamic breakup of micrometer-sized water droplets, J. Phys. Chem. A, 112, 13352–13363, 2008.

Table 1. Overview of the ion (≤2 nm) concentrations measured at closest range of the WFs and at control places (CP).

WF name	Average WF ion conc. [ions m^{-3}]		Max. WF ion conc. [ions m^{-3}]		Average ion conc. at ref. site [ions m^{-3}]		Conc. increase n_{WF}^{-}/n_{CP}^{-}	Conc. increase n_{WF}^{+}/n_{CP}^{+}
	negative	positive	negative	positive	negative	positive		
Krimml	16581	1040	27540	1736	460	390	36	3
Stuiben	43913	2142	54359	3098	546	620	80	3
Bad Gastein	24748	1290	31606	428	774	510	32	3
Gartl	42660	1798	57510	2400	840	760	51	2
Artificial	3294	1446	6251	1582	306	544	11	3
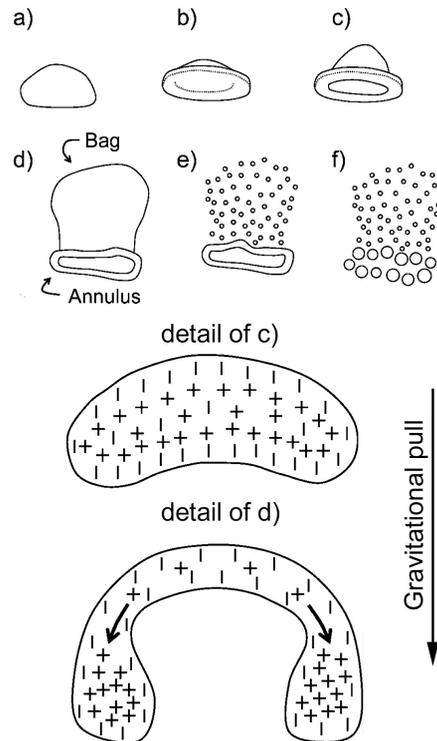
Fig. 1. Theoretical concept of the charge separation mechanism of a falling water droplet. Water bag formation **(a–d)**, fracture into micro-bubbles **(e–f)** (modified according to Zilch et al., 2008).

Fig. 2. Air ion detectors (left), SMPS, anemometer and GPS (middle) and field strength meter.

Fig. 3. Artificial WF at the river Möll.

Fig. 4. The last of three cascades at the Krimml WF.

Title Page

Abstract　Introduction

Conclusions　References

Tables　Figures

◄◄　►►

◄　►

Back　Close

Full Screen / Esc

Printer-friendly Version

Interactive Discussion
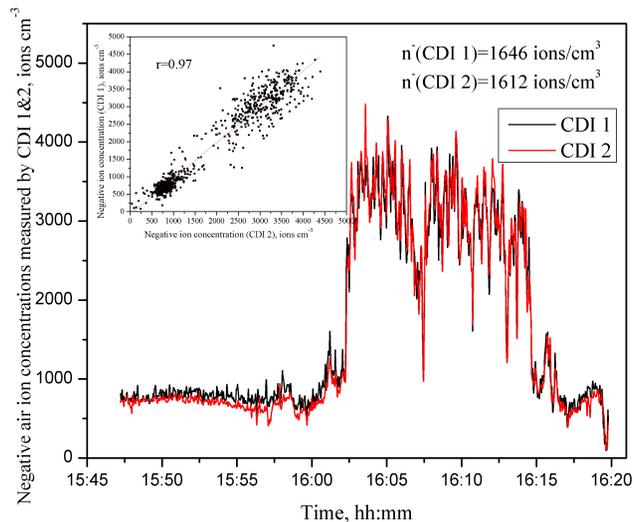
Fig. 5. Intercomparison of ion detectors (CDI-06) nearby Krimml WF versus time. Correlation factor 0.97.
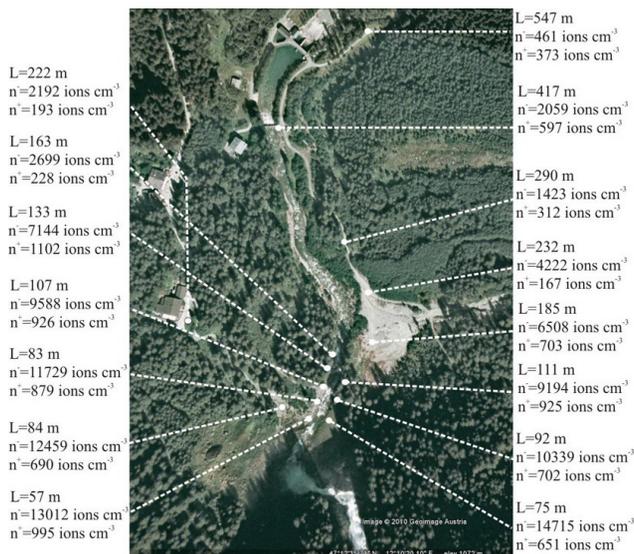
Fig. 6. Three-year summer average of 2 nm ion concentration gradients on both sides of the Krimml WF. The distances from the WF were measured via GPS and visualized on a Google Earth map.

Labels on the left side of the figure:

L=222 m
n^-=2192 ions cm^{-3}
n^+=193 ions cm^{-3}

L=163 m
n^-=2699 ions cm^{-3}
n^+=228 ions cm^{-3}

L=133 m
n^-=7144 ions cm^{-3}
n^+=1102 ions cm^{-3}

L=107 m
n^-=9588 ions cm^{-3}
n^+=926 ions cm^{-3}

L=83 m
n^-=11729 ions cm^{-3}
n^+=879 ions cm^{-3}

L=84 m
n^-=12459 ions cm^{-3}
n^+=690 ions cm^{-3}

L=57 m
n^-=13012 ions cm^{-3}
n^+=995 ions cm^{-3}

Labels on the right side of the figure:

L=547 m
n^-=461 ions cm^{-3}
n^+=373 ions cm^{-3}

L=417 m
n^-=2059 ions cm^{-3}
n^+=597 ions cm^{-3}

L=290 m
n^-=1423 ions cm^{-3}
n^+=312 ions cm^{-3}

L=232 m
n^-=4222 ions cm^{-3}
n^+=167 ions cm^{-3}

L=185 m
n^-=6508 ions cm^{-3}
n^+=703 ions cm^{-3}

L=111 m
n^-=9194 ions cm^{-3}
n^+=925 ions cm^{-3}

L=92 m
n^-=10339 ions cm^{-3}
n^+=702 ions cm^{-3}

L=75 m
n^-=14715 ions cm^{-3}
n^+=651 ions cm^{-3}

Image © 2010 Geoimage Austria
47°12′35.48″N 12°10′20.10″E elev 1072 m
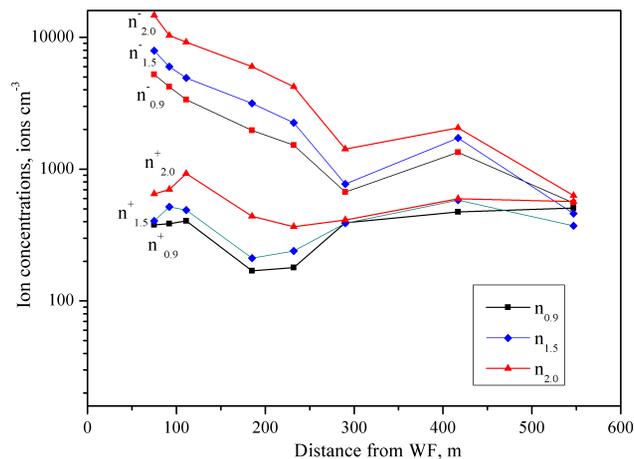
Fig. 7. Integral ion concentrations gradients by ion diameter and polarity measured on the orographic right side of the Krimml WF versus distance.
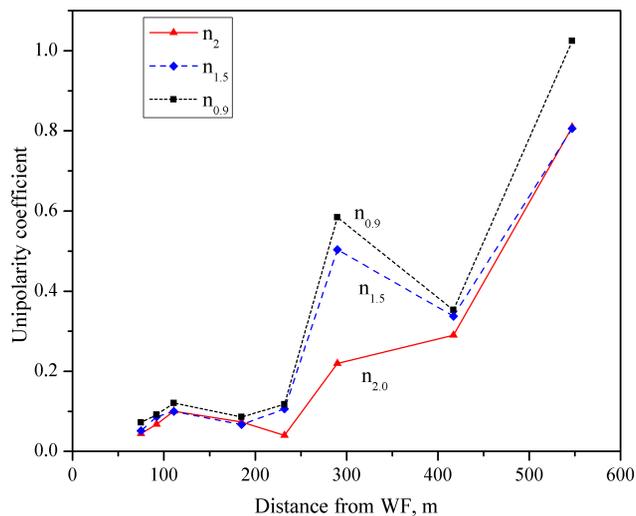
Fig. 8. Unipolarity coefficients for 3 different ion sizes versus distance measured at the Krimml WF.

Fig. 9. Air ion concentrations vs. size for different distance measuring points at Krimml WF. Shaded area indicates interpolated values (cubic B-spline) between CDI-06 (0.9–2.0 nm) and SMPS (5.5–350 nm) measurements. The 547 m data series (magenta curve) represents the reference site where no WF generated ions were expected to occur.

Fig. 10. Gartl WF with surroundings.
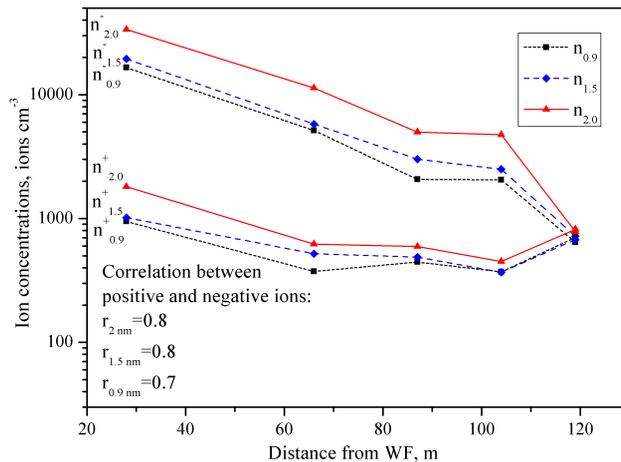
Fig. 11. Integral ion concentration gradients for ion diameter and polarity versus distance at the Gartl WF.
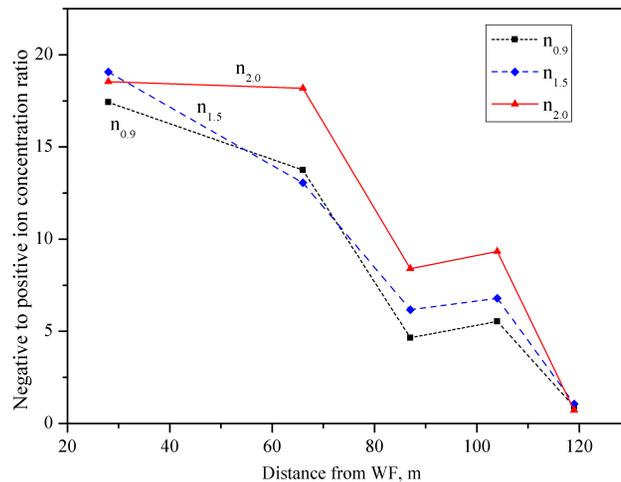
Fig. 12. Negative and positive ion concentration ratios versus distance at the Gartl WF.
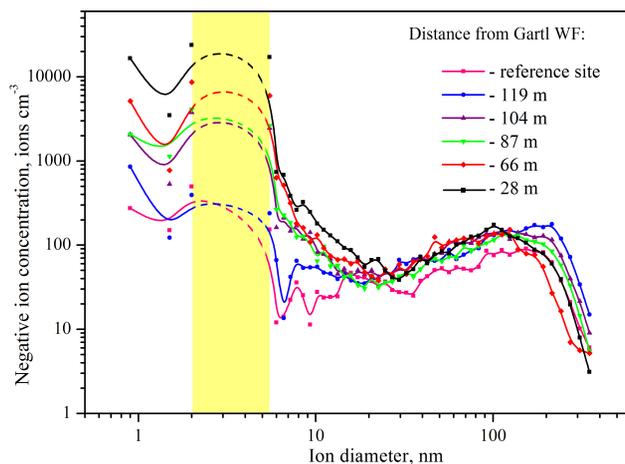
Fig. 13. Air ion concentrations vs. size for different distance measuring points at Gartl WF, Döllach. Shaded area indicates interpolated values (cubic B-spline) between CDI-06 (0.9–2.0 nm) and SMPS (5.5–350 nm) measurements. The reference site data series (magenta curve) represents the reference site where no WF generated ions were expected to occur.